Magnetic Resonance in Solids

Electronic Journal

Invited Editor of Special Issue[‡]: Eduard Baibekov (KFU, Kazan)

Paramagnetic impurity centers of Fe^{3+} in the silicon positions of yttrium orthosilicate

V.A. Vazhenin[1,*], M.Yu. Artyomov[1] A.P. Potapov[1], K.A. Subbotin[2] D.A. Lis[2], S.K. Pavlov[2], A.V. Fokin[1], P.A. Volkov[3]

[1]Ural Federal University, Yekaterinburg 620002, Russia

[2]Prokhorov General Physics Institute of Russian Academy of Sciences, Moscow 119991, Russia

[3]National Research Centre "Kurchatov Institute", Moscow 123182, Russia

E-mail: Vladimir.Vazhenin@urfu.ru

In the Y_2SiO_5 single crystal doped with iron, transitions of three triclinic Fe^{3+} centers localized in silicon positions were detected near $g = 4.3$. The positions of these transitions weakly depend on the orientation of the magnetic field. The orientation behavior of other transitions of these centers has been studied. The parameters of the constructed spin Hamiltonians of two of them in the main axes satisfy the conditions: $b_2^0 \equiv D$ is close to $b_2^2 \equiv 3E$ while $b_2^0 \gg g\beta B$. These centers can be attributed to Fe^{3+} ions localized in silicon positions and compensated for both locally and non-locally by oxygen vacancies.

PACS: 76.30.-v, 76.30.Fc

Keywords: yttrium orthosilicate, impurity ions, paramagnetic resonance

Dedicated to Boris Malkin,
on the occasion of his 85th birthday

1. Introduction

It is important to have information about the composition and concentration of uncontrolled impurities that significantly affect the properties of the material when creating modern materials for quantum electronics. Electron Paramagnetic Resonance (EPR) is an informative method for detecting transitional and rare-earth impurity elements in crystals. It is sensitive to their valence states and structural localizations. In particular, it concerns divalent and trivalent iron ions, which are the most important accidental impurity in many crystals. They are difficult to get rid of and can in many cases seriously deteriorate the luminescent and other characteristics of the material. To implement such diagnostics, reliable information about the EPR spectra of impurity centers in crystals relevant for the aforementioned applications is necessary.

Monoclinic crystals M_2SiO_5 (M = Y, Sc) doped with rare-earth ions are actively studied using magnetic resonance methods as potential candidates for quantum information processing [1–6]. The same crystals with an admixture of Ce^{3+} ions are effective scintillation materials [7–9]. Yttrium orthosilicate doped with chromium ions is considered as the active medium of solid-state lasers generating radiation in the telecommunication spectral range [10, 11] as well as a saturable absorber for passive Q-switching of neodymium and ytterbium lasers [12].

In [13], we previously observed narrow intense EPR signals of two gadolinium centers (Gd1 and Gd2 [14]), along with less intense but broader lines of two iron centers (Fe^{3+}-1 and Fe^{3+}-2) and very weak hyperfine quartets of copper centers ($^{63}Cu^{2+}$ and $^{65}Cu^{2+}$) in a Y_2SiO_5 single crystal doped with iron ions. The centers of iron (Fe^{3+}-1 and Fe^{3+}-2) and copper were studied and described using the spin Hamiltonian formalism, and their localization in the crystal was discussed [13]. The gadolinium and iron centers in the Sc_2SiO_5 crystal isostructural to yttrium orthosilicate were studied in [15].

Magnetic Resonance in Solids. Electronic Journal. 2024, Vol. 26, No 2, 24217 (11 pp.)

1

In addition to the listed centers, in the indicated yttrium silicate samples, we were able to detect three more weak signals (Fig. 1), the positions of which are close to $g = 4.3$ and weakly depend on the orientation of the magnetic field (Fig. 2). Such positions and the orientation behavior of these EPR signals can be explained by the presence in Y_2SiO_5 of triclinic Fe^{3+} centers with an electron spin of $S = 5/2$ and a large zero-field splitting (ZFS). Further in the text, we will call these centers Fe^{3+}-3a, Fe^{3+}-3b, and Fe^{3+}-3c.

Similar centers were previously observed in $CaWO_4$ crystals by the authors [16–20]. These studies showed that the observed nearly isotropic EPR signal is caused by the transition in the middle Kramer's doublet (3↔4) of the Fe^{3+} center, assuming approximately equal parameters of the spin Hamiltonian (SH) [17] $b_2^0 \equiv D$ and $b_2^2 \equiv 3E$, where $b_2^0 \gg g\beta B$ and the values of the fourth-rank fine structure parameters are small. In this case, the transition in the lower doublet (for $b_2^0 > 0$) is forbidden, while in the upper doublet it is predicted in very high fields. In the coordinate system rotated by 90° around the y-axis, the conditions appear as follows: $b_2^2 \gg g\beta B$, $b_2^0 \approx 0$ [21].

Also, similar spectra were found in crystals of molybdate [22] and lead tungstate [23]. The authors of [23] studied the EPR of triclinic centers of uncontrolled impurity of iron ions in $PbWO_4$, localized in the Pb^{2+} position and associated with a vacancy in the lead sublattice. The noticeable difference in the values of the parameters b_2^0 and b_2^2 in the local coordinate system, despite the large zero-field splitting (80 and 150 GHz), also made it possible to detect the transition in the lower doublet ($b_2^0 > 0$) [23]. Furthermore, the literature contains a vast number of reports on the observation of EPR signals with $g = 4.3$ in glasses, frozen solutions, and in some polycrystalline biological systems (see [24] and monograph [25]). This work presents a study of the aforementioned three previously unstudied paramagnetic iron centers in the yttrium orthosilicate crystal.

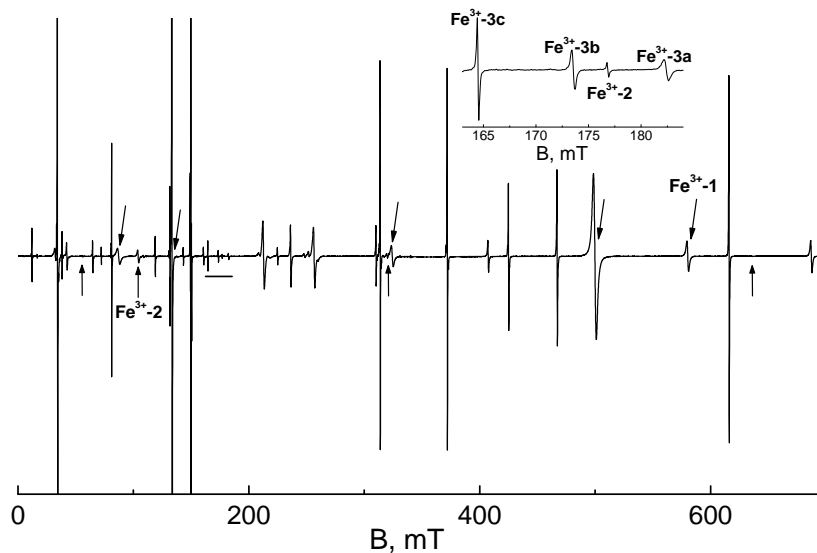**Figure 1.** EPR spectrum of the Y_2SiO_5:Fe crystal in the $\mathbf{B} \parallel b$ orientation ($\mathbf{B}$ is a magnetic field induction) at room temperature and a frequency of 9813 MHz. The upper arrows indicate signals from the Fe^{3+}-1 center, the lower ones are Fe^{3+}-2, and the other intense signals belong to gadolinium centers. The inset shows an enlarged section of the spectrum, marked with a horizontal line.

2. Samples and Experimental Characteristics

In this study, a Y_2SiO_5:Fe single crystal grown by the Czochralski method with a nominal (charge) concentration of iron of 0.4 wt.% (approximately 1 at.% relative to the content of Y) was investigated. Details of the charge preparation and growth conditions are provided in [13].

The grown crystal was almost colorless but not uniformly colored: a barely perceptible bluish tint was visible on the top, while a yellowish hue was on the bottom. After growth, the crystal was additionally annealed in air in a muffle furnace at a temperature of 900°C for 3 weeks to relieve thermal stresses and restore oxygen stoichiometry. After annealing, the crystal acquired a uniform, barely noticeable yellowish coloration.
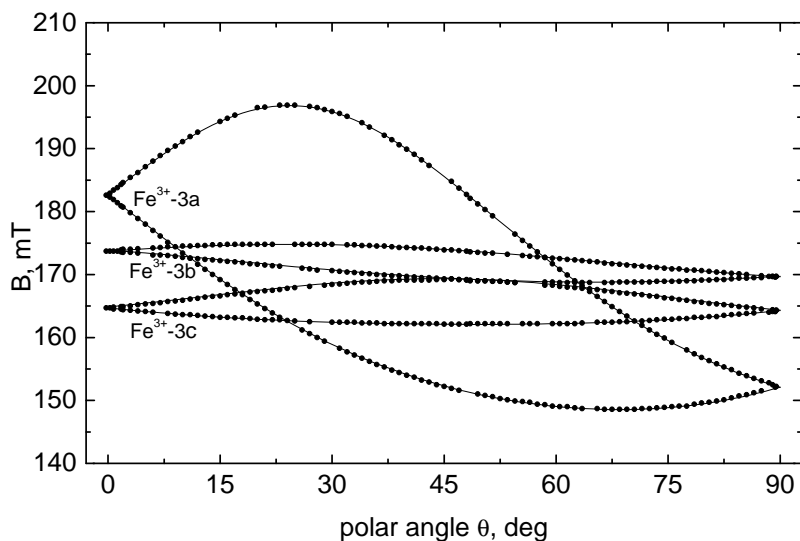
Figure 2. Polar angular dependence of the positions of the $3\leftrightarrow4$ transitions of the Fe^{3+}-3a, Fe^{3+}-3b, and Fe^{3+}-3c centers in the Y_2SiO_5:Fe crystal at $\phi = 23°$ and a frequency of 9812 MHz. The curves are calculated using the parameters from Table 2.

The actual content of impurities in the obtained crystal was measured by the method of mass spectrometry with inductively coupled plasma on an Elan DRC 2 mass spectrometer, Perkin Elmer, USA. Sample collection was performed by the method of laser ablation using the NWR 213 laser ablation system, ESI, USA. A set of NIST 610, 612 standard samples was used as standards for constructing the calibration dependence, and silicon was used as an internal standard.

The measurement results for the most significant impurities are presented in Table 1, with the content of other impurity elements being less than 1 ppm. The measured actual concentration of iron was 19.4 wt. ppm ($1.9 \cdot 10^{-3}$ wt. %). Dividing this value by the nominal charge concentration of iron allows for an estimation of the segregation coefficient of iron between the Y_2SiO_5:Fe crystal and the melt, which was slightly less than 0.005. A previously measured similar quantity for Y_2SiO_5: Cr^{3+} was approximately an order of magnitude larger [26].

The copper content in the crystal turned out to be below the sensitivity limits of the measurement methods used (Table 1). However, in [13], a weak spectrum of two physically nonequivalent paramagnetic Cu^{2+} centers was recorded using the EPR method. For one of them the orientational behavior of the transition positions was measured and the spin Hamiltonian was constructed.

Table 1. Concentration of impurity elements in a Y$_2$SiO$_5$ single crystal doped with iron ions.

Element	Content (wt. ppm)
Al	7.1
Fe	19.4
Ni	1.7
Cu	0
Gd	6.7

According to studies [27–29], the crystal structure of Y$_2$SiO$_5$ belongs to the monoclinic crystal system, space group C$_2$/c (with lattice constants $a = 1.041$ nm, $b = 0.672$ nm, $c = 1.249$ nm and $\beta = 102.65°$.

All atoms in the structure have triclinic local symmetry 1 (C$_1$): silicon is in a distorted oxygen tetrahedron, and Y^{3+} ions occupy two nonequivalent positions with coordination numbers of 6 (M1) and 7 (M2). Each atomic position is multiplied by the elements of symmetry of the crystal structure (inversion center and axis C$_2 \parallel$ b) to four. As a result, when a paramagnetic ion is localized in any of the three positions (M1, M2, Si), two magnetically nonequivalent spectra will be observed in EPR. If the vector of the magnetic field induction **B** lies in the crystallographic ac plane or is parallel to the crystallographic b-axis, these two spectra become equivalent.

The orientation behavior of the EPR transition positions was measured by rotating the magnetic field in the ac planes (azimuthal dependence) and from the b-axis to the ac plane (polar dependence). An orthogonal laboratory coordinate system (CS) xyz [13] was used. In this system, $\mathbf{z} \parallel \mathbf{b}$, and the x and y axes lie in the ac plane. The angle between the x and c axes is about 95° [13].

The measurements of the orientation behavior of the EPR spectra were conducted at room temperature on a Bruker EMX Plus X-band spectrometer in fields up to 1.41 T. The sample in the spectrometer cavity was attached to a holder fixed on the rod of the standard automatic goniometer, capable of rotating around an axis perpendicular to the rod. The sample was cut from a single crystal, oriented relative to the axes of the optical indicatrix (one of these axes coincides with the crystallographic b-axis, the other two lie in the ac plane), and had dimensions of $6 \times 6 \times 1$ mm^3 with the crystallographic b-axis lying in the plane of the square and orthogonal to its side.

3. Results and Discussion

Polar and azimuthal dependencies of the positions of three signals observed near $g = 4.3$ (Fig. 2) and presumably caused by the 3↔4 transitions of Fe^{3+} centers with large ZFS were measured. Fragments of the orientational behavior of other resonances were also measured, but these could not be attributed either to the transitions of Gd^{3+}, Fe^{3+}-1, or Fe^{3+}-2 centers, which was challenging due to the dense spectrum (see Fig. 1), especially in arbitrary orientations of the magnetic field.

To describe the orientational behavior of the transitions of the Fe^{3+}-3a, Fe^{3+}-3b, and Fe^{3+}-3c centers, the spin Hamiltonian (SH) of triclinic symmetry was used [30]:

$$H_{\text{sp}} = \beta(\mathbf{B}g\mathbf{S}) + \frac{1}{3}\sum_m \left(b_2^m O_2^m + c_2^m \Omega_2^m\right) + \frac{1}{60}\sum_m \left(b_4^m O_4^m + c_4^m \Omega_4^m\right), \tag{1}$$

where g is the g-tensor, β is the Bohr magneton, O_n^m, Ω_n^m are the Stevens spin operators, b_n^m,

4

Magnetic Resonance in Solids. Electronic Journal. 2024, Vol. 26, No 2, 24217 (11 pp.)

c_n^m are the fine structure parameters.
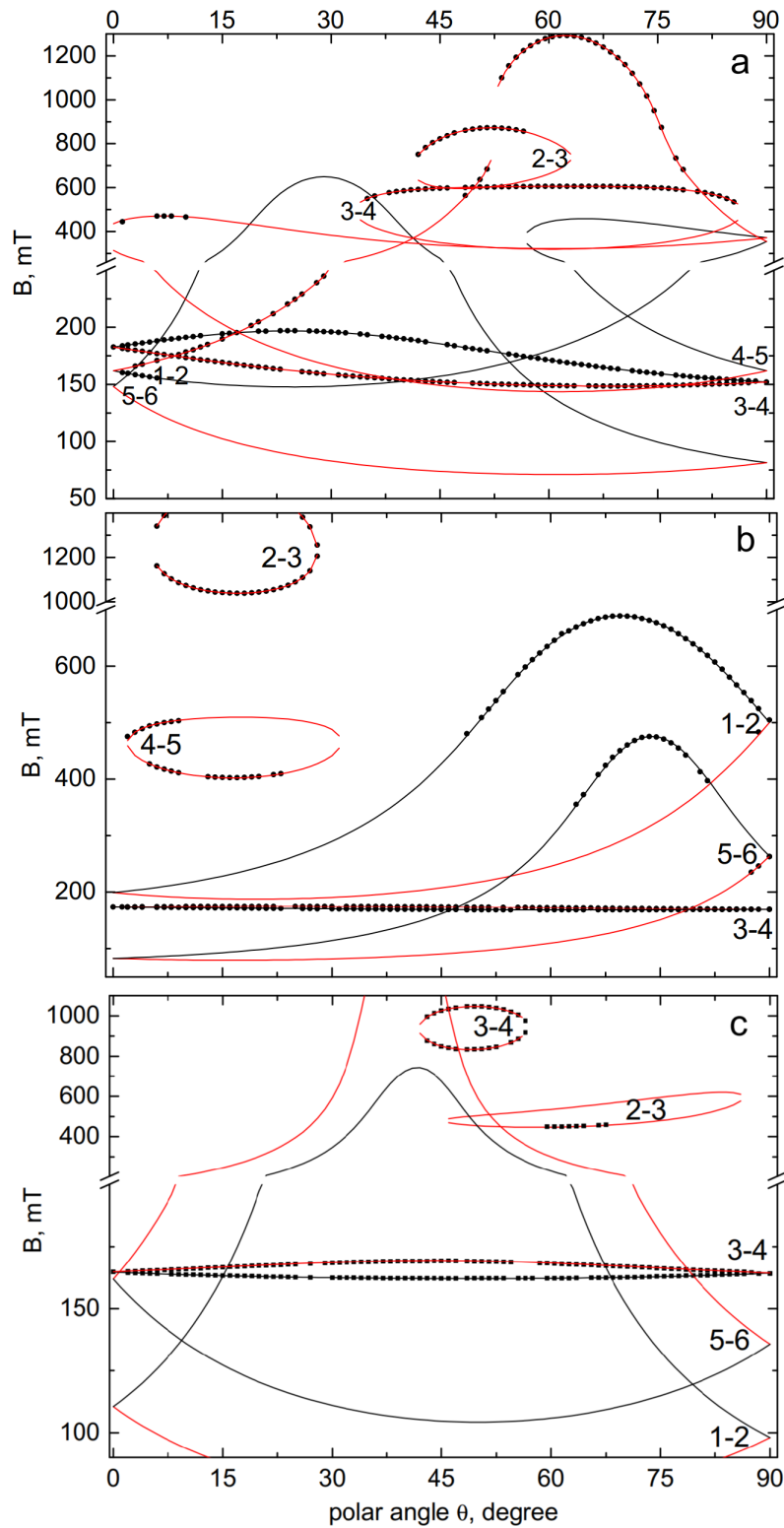
Figure 3. Polar angular dependence of the positions of transitions for centers (a) Fe^{3+}-3a, (b) Fe^{3+}-3b, and (c) Fe^{3+}-3c in Y_2SiO_5 at $\phi = 23°$ and a frequency of 9812 MHz. Points represent experimental data, and curves are calculations with parameters from Table 2. Black and red curves correspond to centers connected by the operation $C_2 \parallel b$.

By minimizing the standard deviation F of the calculated positions (by diagonalizing the

sixth-order complex matrix without the last term SH and considering $g = 2$) from the measured positions of signals 3↔4, we obtained many sets of parameters for different initial values.

Naturally, sets with small values of F, demonstrating zero-field splitting in the tens of GHz, were selected for further work. The obtained sets of parameters were used to calculate the orientational behavior of other transitions, including inter-doublet ones. In cases where unidentified experimental fragments of dependencies were close to the calculated curves, these points were added to the data array and an optimization of the SH parameter set was conducted, including the last term in expression (1). Then, a search for correlation with the calculation of the following unidentified experimental dependencies was carried out, and so on, until exhausting suitable fragments.

The results of optimizing the SH parameters for three centers Fe^{3+}-3(a,b,c) are presented in Table 2. As expected, the ZFS were found to be in the order of tens of GHz. The description of the experimental dependencies in Figures 3-4 by the calculated curves with the parameters listed in Table 2 is quite adequate. The absence of experimental points near some curves is due to the very low probability of transition or the overlap of the indicated spectral region by an intense signal from another center.

Table 3 presents the SH parameters for three centers Fe^{3+}-3(a,b,c) in Y_2SiO_5 in local coordinate systems (in principal axes) of the second-rank fine structure tensors (in MHz). The signs of b_n^m and c_n^m with odd m correspond to one of the magnetically nonequivalent centers. The transition from the laboratory CS to the principal axes system is carried out by sequential rotations (in zyz convention) by Euler angles (in degrees): 20.4, 61.1, 32.2 for Fe^{3+}-3a, 120.8, 110.9, 17.8 for Fe^{3+}-3b, 149.1, 64.1, 43.4 for Fe^{3+}-3c. The principal axes of the fourth-rank tensor were not determined due to the large error of the obtained components. As can be seen, the positions of the 3↔4 transition of the Fe^{3+}-3b and Fe^{3+}-3c centers that have a large ZFS, as well as almost equal values of $|b_2^0|$ and $|b_2^2|$ (in principal axes) depend very little on the orientation of the magnetic field (see Table 3 and Figs. 3-4).

The EPR spectra of Fe^{3+} ions localized in both nonequivalent yttrium positions in the Y_2SiO_5 crystal (Fe^{3+}-1 and Fe^{3+}-2) are well characterized in the study [13]. Therefore, for Fe^{3+}-3(a,b,c) centers, the only place of localization remains the position of silicon Si^{4+} in a distorted oxygen tetrahedron. The difference between the three Fe^{3+}-3(a,b,c) centers is apparently due to different mechanisms of charge compensation for the excess effective negative charge of iron ions in a given position. The compensator is most likely an oxygen vacancy V_O, which has a double excess effective positive charge.

In Y_2SiO_5, all observed Fe^{3+} centers are triclinic, which complicates their identification. However, one should expect the presence of a center with non-local compensation, especially considering that the proposed V_O defect compensates for the charge of two paramagnetic ions simultaneously. In this case, one Fe^{3+} ion can be compensated locally by the oxygen vacancy, forming an associate of the $[Fe-V_O]^+$ type, while the second iron ion would be compensated non-locally. Furthermore, one should expect the formation of several disturbed centers with local compensation, demonstrating fine structure parameters that are distinct from those of the non-locally compensated center and relatively close to each other. The situation where paramagnetic ions form significant concentrations of paired (for example, of the type $[Fe-V_O-Fe]^0$) or more complex aggregates of paramagnetic centers occurs rarely. Moreover, such associates are not described by a single-particle spin Hamiltonian, as demonstrated in [31, 32] using the example of rare-earth ions in forsterite Mg_2SiO_4.
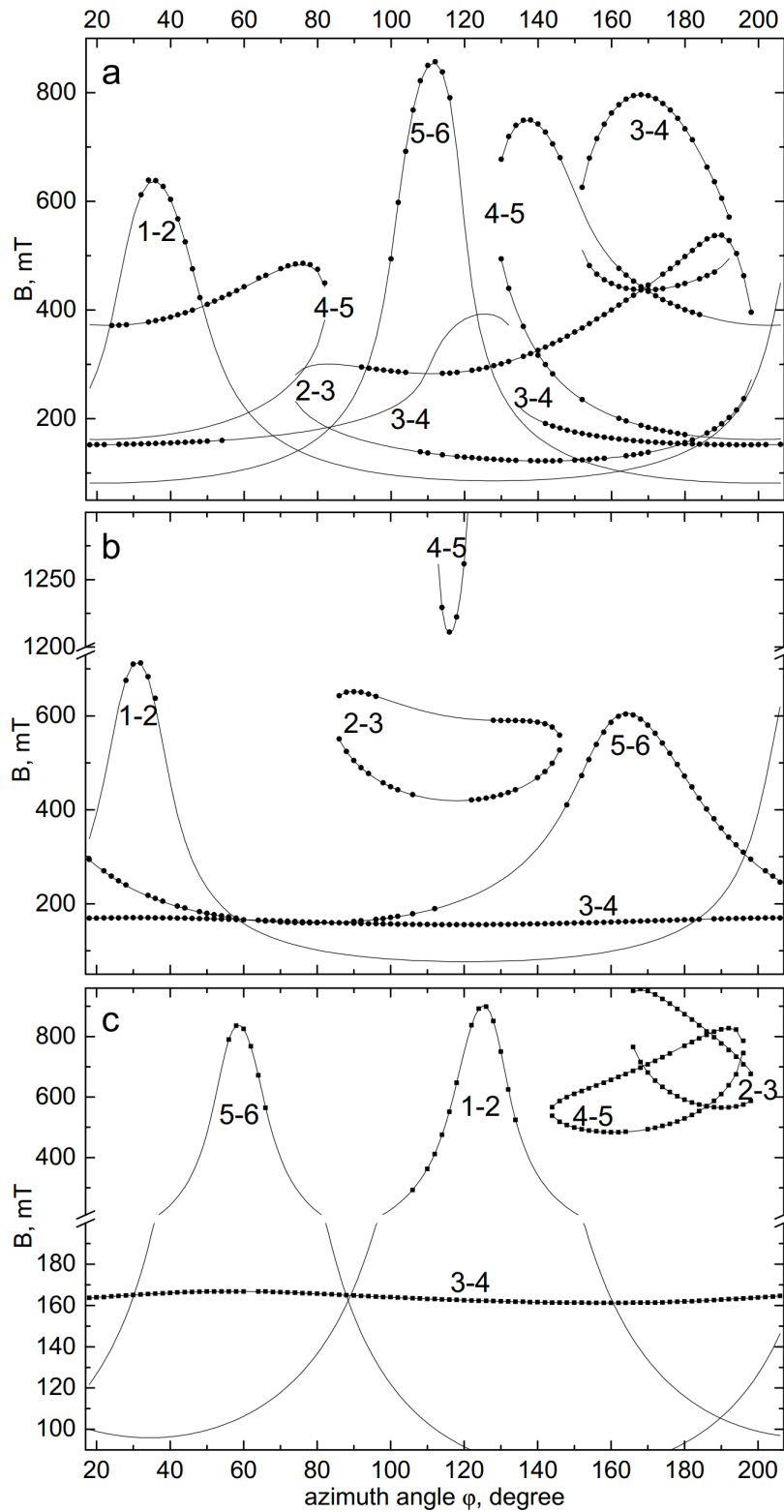
Figure 4. The orientational behavior of the positions of transitions for centers (a) Fe^{3+}-3a, (b) Fe^{3+}-3b, and (c) Fe^{3+}-3c in the ac plane at a frequency of 9812 MHz. Points represent experimental data, and curves are calculations with parameters from Table 2.

Therefore, taking into account the data in Table. 3, it can be assumed that the Fe^{3+}-3a centers should be considered isolated Fe^{3+} ions in the silicon position, and Fe^{3+}-3b and Fe^{3+}-3c as Fe^{3+}-V_O associates. The significant difference between the parameters of the SH associates

Table 2. SH parameters for three centers Fe^{3+}-3(a,b,c) in Y_2SiO_5 in the coordinate system $\mathbf{z}||\mathbf{b}$. Double signs at b_n^m, c_n^m with odd m correspond to two centers connected by the operation $\mathbf{C}_2||\mathbf{b}$. The absolute signs of the parameters were not determined. The values of b_n^m, c_n^m and the root mean square deviation $F(N)$ are given in MHz, N is the number of experimental values used in the optimization procedure.

Parameters	Fe^{3+}-3a	Fe^{3+}-3b	Fe^{3+}-3c
g_x	2.002(1)	2.002(1)	2.002(1)
g_y	2.005(1)	2.002(1)	2.002(1)
g_z	2.003(1)	1.999(1)	2.003(1)
b_2^0	-220(7)	8260(4)	$-3420(10)$
b_2^1	$\pm17000(12)$	$\mp6510(18)$	$\mp42650(20)$
b_2^2	5480(7)	3930(10)	2870(10)
b_4^0	7(5)	9(10)	$-10(6)$
b_4^1	$\pm250(27)$	$\pm520(31)$	$\pm40(40)$
b_4^2	210(25)	150(27)	245(30)
b_4^3	$\mp280(80)$	$\pm90(80)$	$\pm1270(100)$
b_4^4	290(36)	150(32)	$-100(50)$
c_2^1	$\mp1680(15)$	$\pm35150(22)$	$\mp3100(15)$
c_2^2	7460(9)	12270(10)	$-18040(10)$
c_4^1	$\pm300(30)$	$\mp7(27)$	$\mp440(40)$
c_4^2	200(27)	80(31)	$-10(27)$
c_4^3	$\pm350(85)$	$\pm540(120)$	$\pm700(70)$
c_4^4	$-270(36)$	$-110(27)$	$-390(27)$
F(N)	14 (394)	20 (387)	10 (275)
ZFS, GHz	19.5; 24.8	49.7; 42.9	52.2; 49.0

Table 3. SH parameters for three centers Fe^{3+}-3(a,b,c) in Y_2SiO_5 in local coordinate systems (in principal axes) of the second-rank fine structure tensors (in MHz). The signs of b_n^m and c_n^m with odd m correspond to one of the magnetically nonequivalent centers. The absolute values of the parameters b_2^1, c_2^1, c_2^2 are less than 0.004 MHz.

Parameters	Fe^{3+}-3a	Fe^{3+}-3b	Fe^{3+}-3c
b_2^0	6730	-13670	14590
b_2^2	4750	11400	-13690
b_4^0	-20	-40	90
b_4^1	-490	-220	-190
b_4^2	-130	20	-20
b_4^3	-160	1040	1090
b_4^4	-260	120	-110
c_4^1	160	-210	-180
c_4^2	-150	-10	-70
c_4^3	730	320	-1160
c_4^4	120	230	-170
$|b_2^0/b_2^2|$	1.40	1.2	1.07

Fe^{3+}-3b and Fe^{3+}-3c from the corresponding characteristics of Fe^{3+}-3a (Table 3) indicates that the compensating defects are located quite close to the paramagnetic ion. Perhaps even in the

first coordination sphere (approximately $1.6\,\text{Å}$) of the iron ion.

However, in this case, the difference in orientations of the Fe^{3+}-O^- bonds suggests the emergence of not two, but four locally compensated centers. Moreover, according to [33], tetragonal Fe^{3+} centers in $SrTiO_3$ with a vacancy in the nearest oxygen octahedron (approximately $1.95\,\text{Å}$) demonstrate a record value of $D = b_2^0 \gg 43\,\text{GHz}$, which significantly larger then given in Table 3 values for iron ion in the tetrahedron.

In the Y_2SiO_5 structure, two oxygen ions O3 and O1 in the second coordination sphere are located at distances of 3.35 and $3.49\,\text{Å}$ with polar angles of $62°$ and $112°$, respectively [27–29] (more distant oxygen ions are located at too significant a distance, exceeding $3.91°$). Meanwhile, the angles between the z-axis of the laboratory CS and the principal axes of the Fe^{3+}-3b and Fe^{3+}-3c centers, according to the obtained Euler angles, are $111°$ and $64°$, respectively. Therefore, it can be assumed that it is precisely the oxygen vacancies in the second coordination sphere of the Fe^{3+} ion in the silicon position that are associated with the centers Fe^{3+}-3b and Fe^{3+}-3c. To definitively resolve the question of the precise structure of these centers, microscopic calculations of the fine structure parameters of Fe^{3+} ions in yttrium silicate are necessary.

4. Conclusion

In Y_2SiO_5 crystals doped with iron, near $g = 4.3$, weak EPR signals of additional centers (Fe^{3+}-3a, Fe^{3+}-3b, Fe^{3+}-3c), representing iron ions in silicon positions and, apparently, associates based on them, have been detected. As a result of processing the polar and azimuthal angular dependences of the positions both of mentioned signals and other transitions of these centers, their spin Hamiltonians parameters have been obtained both in the laboratory CS and in the principal axes. The b_2^0 and b_2^2 parameters of the centers Fe^{3+}-3b, Fe^{3+}-3c in the principal axes turned out to be quite close, and the ZFS significantly larger than $g\beta\mathbf{B}$, which ensured a weak dependence of the positions of the $3 \leftrightarrow 4$ transitions on the orientation of the magnetic field.

A model for these centers is proposed: Fe^{3+}-3a represents an isolated iron ion in the silicon position, while Fe^{3+}-3b and Fe^{3+}-3c are iron ions in the silicon position, locally compensated by oxygen vacancies V_O, located in the second coordination sphere of the environment.

Acknowledgments

References

1. Welinski S., Ferrier A., Afzelius M., Goldner P., *Phys. Rev. B* **94**, 155116 (2016).

2. Sukhanov A. A., Tarasov V. F., Eremina R. M., Yatsyk I. V., Likerov R. F., Shestakov A. V., Zavartsev Y. D., Zagumennyi A. I., Kutovoi S. A., *Appl. Magn. Reson.* **48**, 589 (2017).

3. Eremina R. M., Gavrilova T. P., Yatsyk I. V., Fazlizhanov I. F., Likerov R. F., Shustov V. A., Zavartsev Y. D., Zagumennyi A. I., Kutovoi S. A., *J. Magn. Magn. Mater.* **440**, 13 (2017).

4. Sukhanov A. A., Likerov R. F., Eremina R. M., Yatsyk I. V., Gavrilova T. P., Tarasov V. F., Zavartsev Y. D., Kutovoi S. A., *J. Magn. Reson.* **295**, 12 (2018).

5. Sukhavov A. A., Tarasov V. F., Zavartsev Y. D., Zagumennyi A. I., Kutovoi S. A., *JETP Lett.* **108**, 210 (2018).

6. Eremina R. M., Tarasov V. F., Konov K. B., Gavrilova T. P., Shestakov A. V., Shustov V. A., Kutovoi S. A., Zavartsev Y. D., *Appl. Magn. Reson.* **49**, 53 (2018).

7. Buryi M. A., Laguta V. V., Rosa J., Nikl M., *Radiat. Meas.* **90**, 23 (2016).

8. Laguta V. V., Zorenko Y. V., Buryi M. A., Gorbenko V. V., Zorenko T. V., Mares J. A., Nikl M., *Opt. Mat.* **72**, 833 (2017).

9. Pidol L., Guillot-Noel O., Kahn-Harari A., Viana B., Pelenc D., Gourier D., *J. Phys. Chem. Solids* **67**, 643 (2006).

10. Koetke J., Kück S., Petermann K., Huber G., Cerullo G., Danailov M., Magni V., Qian L. F., Svelto O., *Opt. Commun.* **101**, 195 (1993).

11. Chai B. H. T., Simony Y., Deka C., Zhang X. X., Munin E., Bass M., in *Bass. OSA Proc.*, Vol. 13 (ASSL, 1992) pp. 28–31.

12. Chang C.-K., Chang J.-Y., Kuo Y.-K., in *Proc. SPIE*, Vol. 4914 (2002) pp. 498–509.

13. Artyomov M. Y., Potapov A. P., Subbotin K. A., Vazhenin V. A., Titov A. I., Fokin A. V., Pavlov S. K., Lis O. N., *Phys. Solid State* **66**, 407 (2024).

14. Fokin A. V., Vazhenin V. A., Potapov A. P., Artyomov M. Y., Subbotin K. A., Titov A. I., *Opt. Mat.* **132**, 112741 (2022).

15. Vazhenin V. A., Potapov A. P., Subbotin K. A., Fokin A. V., Artyomov M. Y., Titov A. I., Pavlov S. K., *Phys. Solid State* **65**, 744 (2023).

16. Griffith J. S., *Mol. Phys.* **8**, 217 (1964).

17. Kedzie R. W., Lyons D. H., Kestigian M., *Phys. Rev.* **138**, A918 (1965).

18. Golding R. M., Kestigian M., Tennant C. W., *J. Phys. C: Solid State Phys.* **11**, 5041 (1978).

19. MacGavin D. G., Tennant C. W., *J. Magn. Res.* **61**, 321 (1985).

20. Claridge R. F. C., Tennant C. W., MacGavin D. G., *J. Phys. Chem. Solids* **58**, 813 (1997).

21. Zaripov M. M., *Osnovy teorii spektrov elektronnogo paramagnitnogo rezonansa v kristallakh. Kurs lektsii* (Kazanskii gosuniversitet, 2009) 208 p. [in Russian].

22. Friedrich M., Karthe W., *Phys. Stat. Sol. (b)* **94**, 451 (1979).

23. Asatryan G. R., Nikl M., Vazhenin V. A., Potapov A. P., *Phys. Solid State* **55**, 116 (2013).

24. Garif'yanov N. S., Zaripov M. M., *Fizika Tverdogo Tela* **6**, 1545 (1964), [in Russian].

25. Klyava Y., *EPR-spektroskopiya neuporyadochennykh tverdykh tel* (Zinatne, Riga, 1988) 320 p. [in Russian].

26. Vazhenin V., Potapov A., Subbotin K., Lis D., Artyomov M., Sanina V., Chernova E., Fokin A., *Opt. Mat.* **117**, 111107 (2021).

27. Maksimov B. A., Il'yukhina V. V., Kharitonov Y. A., Belov N. V., *Kristallografiya* **15**, 926 (1970), [in Russian].

28. Anan'eva G., Korovkin A., Merkulyaeva T., Morozova A., Petrov M., Savinova I., Startsev V., Feofilov P., *Inorg. Mater.* **17**, 754 (1981).

29. Leonyuk N. I., Belokoneva E. L., Bocelli G., Righi L., Shvanskii E. V., Henrykhson R. V., Kulman N. V., Kozhbakhteeva D. E., *Cryst. Res. Technol.* **34**, 1175 (1999).

30. Al'tshuler S. A., Kozyrev B. M., *Electron Paramagnetic Resonance in Compounds of Transition Elements*, 2nd ed. (John Wiley & Sons, 1974) 589 p.

31. Gaister A. V., Zharikov E. V., Konovalov A. A., Subbotin K. A., Tarasov V. F., *JETP Lett.* **77**, 625 (2003).

32. Tarasov V. F., Sukhanov A. A., Zharikov E. V., Subbotin K. A., Lis D. A., *Appl. Magn. Reson.* **53**, 1211 (2022).

33. Kirkpatrick E. S., Müller K. A., Rubin R. S., *Phys. Rev.* **135**, A86 (1964).